



Eidgenössische Technische Hochschule Zürich
Swiss Federal Institute of Technology Zurich

Development of an RF resonator for a double junction ion trap

Semester Project

Konstantin Nesterov

Tuesday 23rd April, 2019

Advisors: Prof. Dr. J. Home, Chiara Decaroli

Department of Physics, ETH Zürich

Abstract

In this report I will describe the modeling, designing and testing of an RF helical resonator suitable for delivering RF signal to a double-junction ion trap in a cryogenic environment.

Contents

Contents	ii
1 Introduction	1
1.1 Why do we need resonators?	1
1.2 Context of this project	2
1.3 Kinds of resonators	3
1.3.1 Helical	3
1.3.2 RLC	4
1.3.3 Crystal	4
1.3.4 Choosing the right one	5
2 Theory	7
2.1 What is a resonator?	7
2.2 Helical resonator models	7
2.2.1 Macalpine & Schildknecht	7
2.2.2 Siversn et al.	8
2.3 Comparison	12
3 Design	13
3.1 On a quest to perfect parameters	13
3.1.1 First iteration	13
3.1.2 Precise fit	14
3.2 Shaping the 3D model	16
3.2.1 RF resonator	17
3.2.2 Bottom cap	18
3.2.3 Shield	19
3.2.4 Helix	20
3.2.5 Helix support	21
3.2.6 Top cap	22
3.2.7 Top cap clamp	23

Contents

3.2.8	Antenna mount	24
3.2.9	Antenna	25
3.3	Final assembly	26
4	Validation	27
4.1	Measurements	27
4.2	Analysis	29
4.3	Ideal drive	30
4.4	Power dissipation	33
4.5	Voltage gain	33
5	Results	35
6	Outlook	36
7	Conclusion	37
A	Mathematica code for Macalpine's model	38
B	Mathematica code for Siverns' model	41
	Bibliography	45

Chapter 1

Introduction

Quantum computing is an exciting and rapidly evolving field of modern science. One of the most promising implementations of a quantum computer is based on the ability to control and measure systems of trapped ions. Those ions are typically confined in Paul (RF) [15] traps by applying static and oscillating RF signals to the trap electrodes, which on average generate a confining electric potential.

1.1 Why do we need resonators?

One could potentially couple a radio frequency source directly to an ion's trap. However this creates the following challenges:

- noise from the source may contribute to heating of trapped ions [19],
- in order to maintain efficient cryostat cooling the amount of generated heat within it should be minimized. In order to stabilize ions in the ion trap the confining RF signal must have a reasonably high voltage amplitude. An RF resonator close to the signal consumption area allows to reduce the length of an actively heated (with accordance to the Joule–Lenz law [16]) high voltage wire,
- impedance mismatch between source and trap leads to an additional dissipation of RF power.

These issues can be avoided by placing an amplifier close to the Paul trap, which would filter the incoming signal and output it with a voltage suitable for operating the trap. There are two available options: active and passive amplifiers. The core difference between them is that active amplifiers use an additional power source to increase output power of the signal while passive amplifiers rather modify the shape of the input signal conserving the overall power — in our case the voltage amplitude gain is balanced by the current amplitude decline.

1.2. Context of this project

Active amplifiers perform better in terms of voltage gain at room temperatures. However, the aim of this project is to create a resonator used within a cryogenic environment. The properties of transistors powering active amplifiers depend heavily on a combination of densities of free electrons and holes. Lowering the temperature tends to reduce [2] these densities significantly, turning semiconductors at room temperatures into practically dielectrics.

It leaves us with passive amplifiers (resonators).

1.2 Context of this project

This semester project aims to be a part of an attempt to create a scalable quantum computing architecture by Chiara Decaroli. It provides the following benefits compared to existing solutions:

- using subtractive laser writing to manufacture wafers eliminates misalignment effects by allowing a “self assembly” of different wafers,
- double junction ion trap designed for parallel operations, Decoherence Free Subspace (DFS) ion transport across the junctions, and manipulation of long chains of ions,
- potential integrated laser delivery through optical lensed fibers eliminates the need for bulky optics and custom objectives which limit scalability.

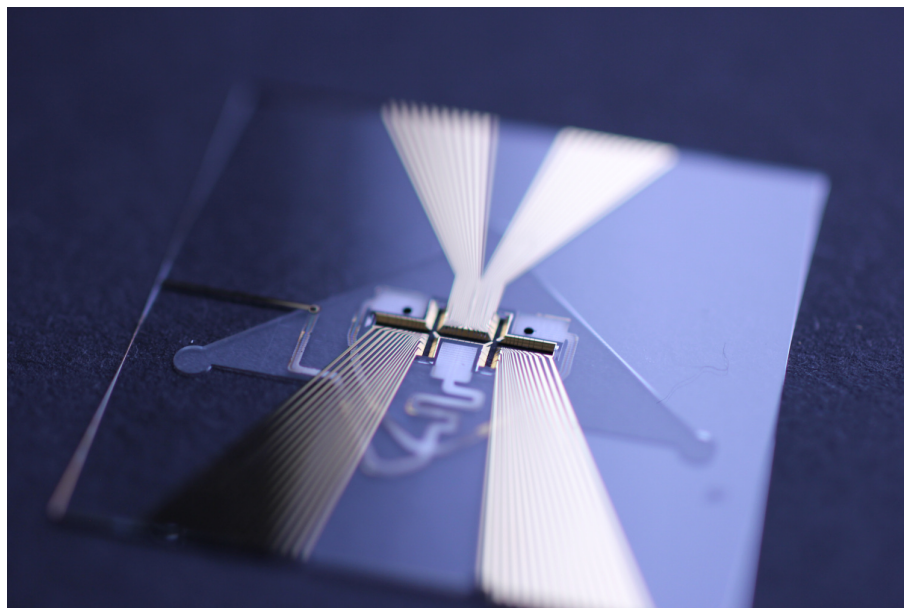


Figure 11: Top wafer of the double junction trap

1.3 Kinds of resonators

The required frequency of 40 MHz limits our selection to the following types of resonators: helical [7, 8, 20, 11, 10] or, for higher frequencies, coaxial [9], RLC [5, 12, 6], and crystal oscillators. Multiple available solutions require us to do an analysis for a reasoned choice.

1.3.1 Helical

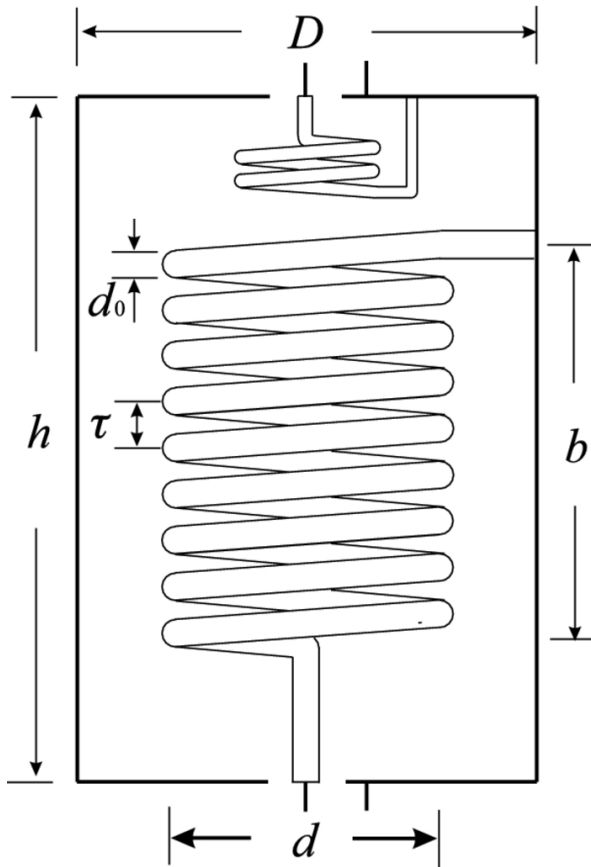


Figure 12: Schematic diagram of a helical resonator indicating shield diameter D , shield height h , coil diameter d , coil height b , winding pitch τ , and coil wire diameter d_0 . [1]

Helical resonators are commonly selected to be coupled with ion traps due to their high quality factors and ability to operate on high frequencies. It is a perfect option for ion traps operated at room temperatures, since in absence of space constraints they are able to provide Q values of a couple of thousands. However in order to achieve those Q , the fabrication process needs to be quite precise to avoid reflections of traveling waves which negatively influence the overall gain.

1.3.2 RLC



Figure 13: Example of a parallel RLC circuit

RLC amplifiers are a convenient choice for space-bounded environments, such as cryostats. Typical implementation pumps energy between two reactive components — inductor and capacitor. Assembly of RLC circuit is easier than of helical resonator since the physical placement of lumped parts does not influence the resulting quality factor. But it also means that the quality of these components is a major factor for successful creation. Given that units' data sheets rarely provide values for cryogenic or vacuum setup it takes a lot of trial and error to find the right ones [5].

1.3.3 Crystal

Unlike helical and RLC resonators, the crystal oscillators do not store energy just in the electric field. This type of resonator utilizes piezoelectric effect to transform applied harmonic voltage into surface mechanical modes and vice versa.

Narrow excitation spectrum is provided by physical dimensions imposing hard constraints on vibrational oscillations and could have made such device an ideal filtering solution for ion traps. Unfortunately, there are some major downsides that seriously limit its applicability:

- after fabrication resonant frequency can not be widely tuned
- limited stability of the crystal does not allow high voltages

1.3.4 Choosing the right one

Summarizing constraints for a resonator within the cryostat:

- Helical
 - Max voltage is limited by the size (we want to avoid electrical breakdown between the helix and the shield), generated thermal power (mainly because of the resistance of the solder joints) and the thickness of the coil wire,
 - Max frequency is limited by the manufacturing complexity — high frequencies in small resonators require the coil to be produced from a very thin wire,
 - Resonant frequency tunability depends on the exact design, is typically crude and is achieved by varying capacitive or inductive coupling between the helix and the antenna.
- RLC
 - Max voltage is limited by the quality of components used and generated thermal power,
 - Max frequency is limited by the quality of components used,
 - Resonant frequency can be fine-tuned by using variable electrical components.
- Crystal
 - Max voltage is limited by the mechanical stability of the crystal,
 - Max frequency — no information,
 - Resonant frequency is almost fixed.

Table 11 gives a more visual explanation of above.

Type	Max voltage	Max frequency	Tunability
Helical	+++	+++	++
RLC	++	++	+++
Crystal	+	?	+

Table 11: Empirical interrelation between parameters of different types of resonators

In our setup, the combination of high voltage and frequency values with our constraints on available space makes helical resonator the optimal option. However, difficulties of assembly do not make it a perfect solution in terms of scalability — for a production-grade setup RLC amplifier might be preferred.

1.3. Kinds of resonators

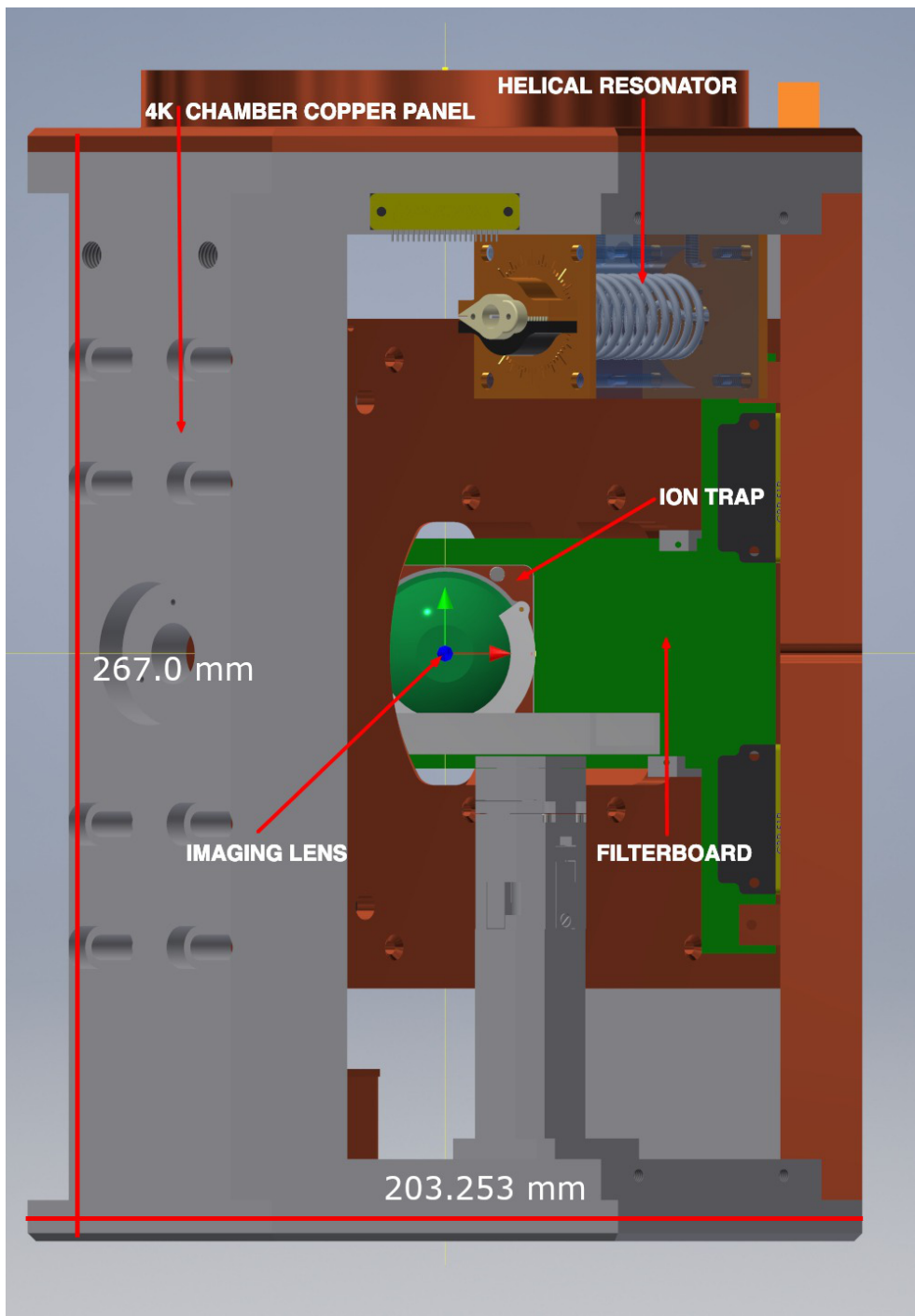


Figure 14: 3D model of the 4K cryostat chamber, design by Roland Matt

Chapter 2

Theory

2.1 What is a resonator?

By resonator we mean a harmonic oscillator within which some quantity varies harmonically with time. In case of a helical resonator an alternating current in electrical circuit periodically transfers the inductive energy stored in a magnetic field of the helix into the capacitive electric field energy between the helix and the shield. When being stimulated by an RF signal with a natural frequency of the system, voltage amplitude grows until the damping mechanisms are strong enough to balance the resonant effect.

2.2 Helical resonator models

In order to create a helical resonator satisfying our experimental conditions and limitations we inevitably come to a need for a theoretical model that would be able to predict the essential characteristics of the resulting unit. The following sections aim to provide an overview and comparison between the models.

2.2.1 Macalpine & Schildknecht

A well-known approach [14] for describing helical resonators was introduced in the same year as Richard Feynman's idea [4] to use quantum systems for computations. It was motivated by the possibility to reduce volume compared to TEM-mode coaxial-line resonators (90% volume reduction for the reference case [14]). While skipping a detailed theoretical analysis it nevertheless provides a basis for constructing a resonator: such as regions of usefulness, design considerations and a set of parameters' dependencies maximizing Q .

2.2. Helical resonator models

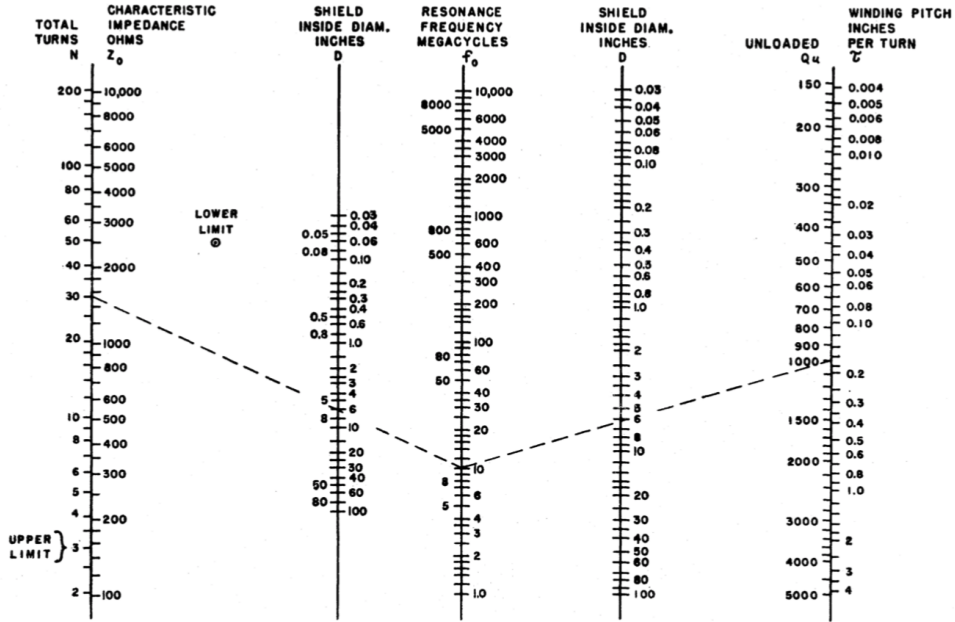


Figure 21: Design chart for quarter-wave helical resonators [14]

While describing essential properties of an unloaded helical quarter-wave resonator, this paper [14] also predicts the shift of resonant frequency if an external load is connected. In order to define a new frequency one can make use of telegraph equations [17] by effectively treating the ion trap as a capacitor.

Important results of [14] can be found in equations 2.1 with parameters named as in the figure 12.

$$\begin{aligned} d/D &= 0.55 \\ b/d &= 1.5 \\ h \approx (b + D/2) \end{aligned} \tag{2.1}$$

2.2.2 Sivers et al.

Unfortunately modeling an ion trap as a pure capacitive load is not always accurate. Introducing resistive losses imposes an additional shift of resonant frequency which pushes the deviation from self-resonant frequency even further. It is possible to tune the strength of the inductive coupling between the antenna and the main coil to compensate this shift while losing in efficiency.

These limitations of Macalpine's & Schildknecht's [14] model have been overcome in a newer paper [18] which takes the development of an amplifier, specifically for the needs of quantum computing, one step further. By taking a look at the joint resonator + ion trap system as a whole it aims to

2.2. Helical resonator models

predict the effective Q and frequency. This model ensures that it's possible to find optimal parameters for given experimental constraints.

While it is heavily recommended to check the original [18] paper to understand the theory behind calculations in appendix B we will provide a short explanation of the exact usage below. All symbols correspond to [18].

In our approach the only varying parameters are the diameter of a shield D and the diameter of a helix d with $\alpha = d/D$.

Formula for Q from [18] depends on the inductance of the coil L_C (2.3), the real part of the total impedance Z_{real} (2.11) and the target frequency ω_0 ($2\pi * 40$ MHz). In the following equations we would expand dependencies until it is possible to express everything through our target and varying parameters.

$$Q = \frac{L_C \omega_0}{Z_{real}} \quad (2.2)$$

Let's start with defining the inductance of the coil L_C . For a long solenoid as modified by the effect of the shield [14] inductance can be described as linearly dependent on the length of the coil b (2.4) and a coefficient K_{L_c} (2.5).

$$L_C = b * K_{L_c} \quad (2.3)$$

The length of the coil b can be derived [14] from the height h (56 mm) and the inner diameter D of the shield. Since D varies resulting b might become less than 0 — this case is handled properly in the appendix B.

$$b = h - D/2 \quad (2.4)$$

The coefficient K_{L_c} depends on the diameter of the helix d , the inner diameter D of the shield and the winding pitch τ (2.7).

$$K_{L_c} = 39.37 \frac{0.025 d^2 (1 - \alpha^2)}{\tau^2} 10^{-6} \text{ H/m} \quad (2.5)$$

We take d_0 from Macalpine's calculations (see appendix A) and define τ as suggested in [14].

$$d_0 = \text{Macalpine's} \quad (2.6)$$

$$\tau = 2 * d_0 \quad (2.7)$$

Looking back at the equation for Q (2.2) we can see that the only undefined part is Z_{real} (2.11). Naturally, first we need to define total impedance Z_{tot} as a sum of the following impedances: coil Z_{coil} (2.9), equivalent Z_E (2.10) and resistances: shield R_s (2.24) and helical coil to shield junction R_j (2.28).

$$Z_{tot} = Z_{coil} + Z_E + R_s + R_j \quad (2.8)$$

2.2. Helical resonator models

The impedance of the coil is dependent on the coil resistivity R_c (2.21) and reactances X_{L_c} (2.12, due to the inductance of the coil) and X_{C_c} (2.13, due to the the coil self-capacitance).

$$Z_{coil} = \left((iX_{L_c} + R_c)^{-1} + (X_{C_c}/i)^{-1} \right)^{-1} \quad (2.9)$$

In order to define the equivalent impedance we use the resistance of the ion trap R_t (expected value of 0.1 Ohm was used) and some reactances, such as X_{C_t} (2.14, caused by the capacitance of the trap), X_{C_w} (2.15, caused by the capacitance of the ion trap connecting wires), and X_{C_s} (2.16, caused by the capacitance between the coil and the shield).

$$Z_E = \left((X_{C_t}/i + R_t)^{-1} + (X_{C_w}/i)^{-1} + (X_{C_s}/i)^{-1} \right)^{-1} \quad (2.10)$$

By substituting equations 2.9 and 2.10 into 2.8 and extracting the real part we can express Z_{real} .

$$\begin{aligned} Z_{real} = & \frac{R_c X_{C_c}^2}{R_c^2 + (X_{C_c} - X_{L_c})^2} \\ & + \frac{R_t X_{C_s} X_{C_w}}{R_t^2 (X_{C_s} + X_{C_w})^2 + (X_{C_s} (X_{C_t} + X_{C_w}) + X_{C_t} X_{C_w})^2} \\ & + R_s + R_j \end{aligned} \quad (2.11)$$

Let us expand all reactances of Z_{real} (2.11). Their definitions would include the target frequency ω_0 , the inductance of the coil L_C (2.3) and a group of capacitances: coil self C_c (2.17), ion trap C_t (varied parameter of 10, 15, 20 pF), ion trap connecting wires C_w (expected value of $1 * 10^{-5}$ pF was used), and coil to shield C_s (2.18).

$$X_{L_c} = \omega_0 L_C \quad (2.12)$$

$$X_{C_c} = (\omega_0 C_c)^{-1} \quad (2.13)$$

$$X_{C_t} = (\omega_0 C_t)^{-1} \quad (2.14)$$

$$X_{C_w} = (\omega_0 C_w)^{-1} \quad (2.15)$$

$$X_{C_s} = (\omega_0 C_s)^{-1} \quad (2.16)$$

The coil self capacitance C_c can be calculated as below.

$$C_c = \left(\left(11.26 \frac{b}{d} \right) + 8 + \left(\frac{27}{\sqrt{b/d}} \right) \right) d \text{ pF} \quad (2.17)$$

2.2. Helical resonator models

In order to express the capacitance between the coil and the shield we use an approach similar to what was used for L_C (2.3) by introducing a coefficient K_{C_s} (2.19).

$$C_s = b * K_{C_s} \quad (2.18)$$

The equation for the multiplier K_{C_s} is shown below.

$$K_{C_s} = 39.37 \frac{0.75}{\log_{10}(D/d)} \text{ pF/m} \quad (2.19)$$

With all capacitances in place the resonant frequency ω_{res} can be found. We only use it to determine whether it is close to the target frequency ω_0 which is actually used in the calculations.

$$\omega_{res} = ((C_s + C_t + C_w + C_c) L_C)^{-1/2} \quad (2.20)$$

In order to complete the derivation of the coil impedance Z_{coil} (2.9) we need to additionally provide a value for the coil resistance R_c . It depends on the copper resistivity ρ ($1.7 * 10^{-8}$ Ohm*m), the unwound length of the coil l_c (2.22), thickness of the coil wire d_0 , and the skin depth of copper δ (2.23, since the current would only flow through the skin region).

$$R_c = \frac{\rho l_c}{d_0 \pi \delta} \quad (2.21)$$

From the geometry of the coil we can express the unwound length through the diameter d , pitch τ , and height b .

$$l_c = 2\pi \sqrt{\left(\frac{d}{2}\right)^2 + \left(\frac{\tau}{2\pi}\right)^2} \frac{b}{\tau} \quad (2.22)$$

Calculations of the skin depth are standard.

$$\delta = \sqrt{\frac{2\rho}{\omega_0 \mu_0}} \quad (2.23)$$

Looking again at the expression for the real part of total impedance Z_{real} (2.11) we see that the only missing parts are the shield R_s (2.24) and helical coil to shield junction R_j (2.28) resistances. Similar to the coil resistance R_c (2.21) we can define R_s by accounting for the coil height b and the "unwound" length l_s (2.25) that the currents take on the shield inner surface.

$$R_s = \frac{\rho l_s}{b \delta} \quad (2.24)$$

2.3. Comparison

The distance of the path l_s in the shield is dependent on the number of "turns" N_s (2.26) the current takes.

$$l_s = N_s \sqrt{\left(\frac{\pi d}{\alpha}\right)^2 + \left(\frac{b}{N_s}\right)^2} \quad (2.25)$$

This number N_s can be defined as below, with r (2.27) being the difference between the coil and inner shield radii.

$$N_s = \frac{b l_c}{4\pi r^2} \quad (2.26)$$

Calculations for the difference between radii r follows naturally from the geometrical considerations.

$$r = \frac{d}{2} (\alpha^{-1} - 1) \quad (2.27)$$

The resistance of the solder joint is dependent on the target frequency ω_0 with $3 * 10^{-3}$ Ohm being a typical resistance value for a DC current.

$$R_j = 0.003 \sqrt{\frac{\omega_0}{2\pi 10^5}} \text{ Ohm} \quad (2.28)$$

With these we have everything required for the expression for Q (2.2).

2.3 Comparison

Macalpine's and Schildknecht's [14] model gives insights for designing a helical quarter-wave resonator with a given self-resonant frequency. However major shifts from it can be expected when connecting the ion trap. Sivers' et al. approach [18] investigates connections between various parameters in the total circuit. As a result one could create a resonator which implements a transfer function closer to a desired one. Considering these benefits the Sivers model [18] was selected.

Chapter 3

Design

This chapter provides a representation of efforts one must face to make a jump from dry theoretical models to a virtually real device.

3.1 On a quest to perfect parameters

Our journey begins with a necessity to define restrictions of the problem. The intended environment would be a 4K cryogenic chamber (figure 14), which imposes dimensions restrictions. The ion trap requires a defined frequency for successful confinement of ions and has a capacitance. Summarized restrictions can be found in table 31.

Parameter	Description	Value
V_{max}	Maximum volume of the resonator	$(60 \text{ mm})^3$
ω_0	Target frequency of the trap	40 MHz
C_{trap}	Capacitance of the trap	10–20 pF

Table 31: Restrictions of a system

3.1.1 First iteration

Siversn's model [18] is dependent on outcomes from Macalpine's model [14] thus one needs to find these beforehand. Exact value of a trap's capacitance is unknown at the moment of calculations so it was decided to use and compare values from a following set of capacitances: $C_{trap} = [10, 15, 20] \text{ pF}$. The modified Macalpine's model, found in the appendix A, also predicts resonant frequency shift when connecting a capacitor. The unloaded frequency needed to be varied until the loaded frequency equals target frequency. Results are provided in table 32, naming is consistent with [14].

Parameter	Value		
	10	15	20
C_{trap} , pF			
B , mm (length of a shield)		60.0	
D , mm (diameter of a shield)		45.0	
b , mm (length of a coil)		37.1	
N_t (number of turns)	11.0	9.2	8.1
d_0 , mm (diameter of a wire)	1.7	2.0	2.3
τ , mm (pitch of a helix)	3.4	4.0	4.6
f_0 , MHz (unloaded frequency)	97.0	116.0	132.8
Q (unloaded quality factor)	873.2	954.8	1022.4

Table 32: Joint output of the appendix A

3.1.2 Precise fit

After defining an approximate region of interest we can proceed to calculations utilizing Siversn's model [18] with implementation provided in the appendix B. Volume requirements were also better clarified with the goal to get the best quality factor by varying coil's parameters. Updated restrictions can be found in the table 33. One could argue that all values of d_0 are lower than the recommended in [18] thickness of 5 mm. This is true and additional measures to handle it can be found in section 3.2.5.

Parameter	Value		
	10	15	20
C_{trap} , pF			
B , mm (length of a shield)		56.0	
D_{max} , mm (max diameter of a shield)		38.0	
d_0 , mm (diameter of a wire)	1.7	2.0	2.3
τ , mm (pitch of a helix)	3.4	4.0	4.6
ω_0 , MHz (resonator frequency)	44.6	45.6	46.9
Q	418	360	311

Table 33: Restrictions for the Siversn's model

Fixed values of the table 33 allow us to independently change 2 remaining parameters — diameter of a shield and diameter of a coil. Appendix's B output of Q values is provided in the figures 31, 32, 33. By selecting a point in a $\{d, \gamma = d/D\}$ space that maximizes Q for a set of C_{trap} values we get final parameters for our RF resonator as defined in the table 34.

Since selected dimensional parameters in the table 34 correspond to those of $C_{trap} = 10$ pF we would expect the unloaded frequency f_0 and the unloaded Q to be equal to ones mentioned in the table 32.

3.1. On a quest to perfect parameters

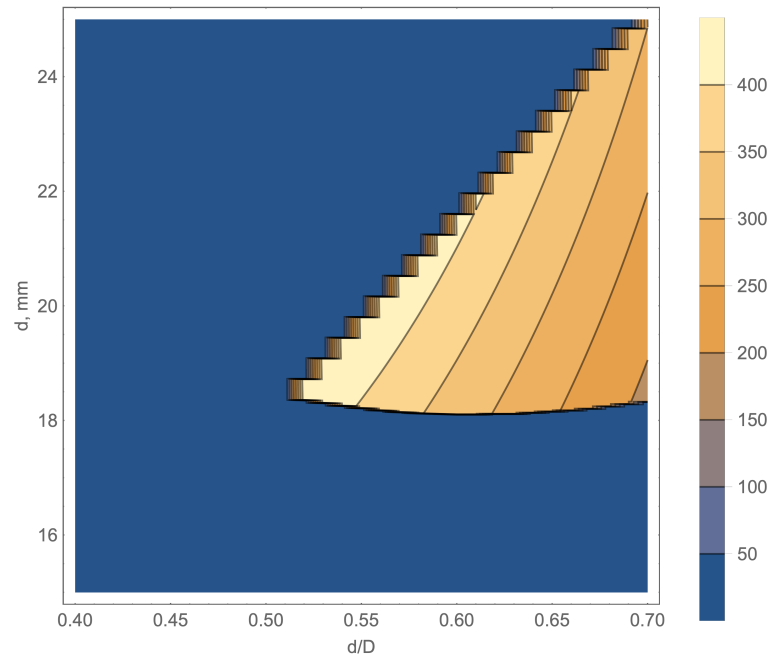


Figure 31: Q values plot for $C_{trap} = 10$ pF

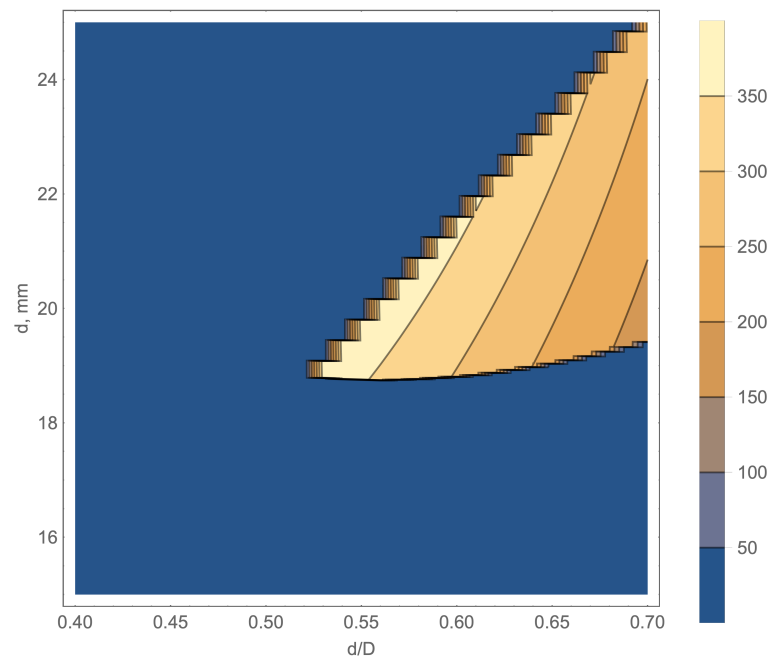


Figure 32: Q values plot for $C_{trap} = 15$ pF

3.2. Shaping the 3D model

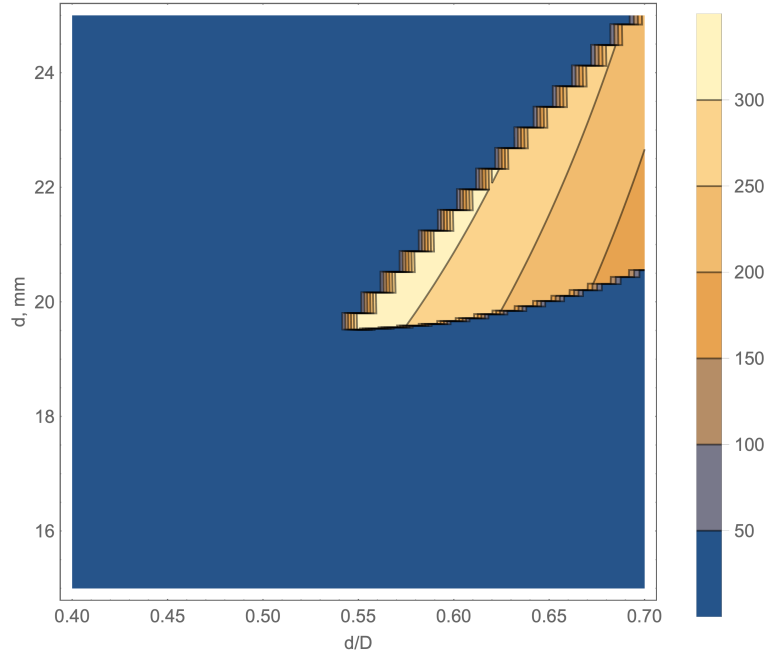


Figure 33: Q values plot for $C_{trap} = 20 \text{ pF}$

Parameter	Value
B , mm (length of a shield)	56.0
D , mm (diameter of a shield)	34.5
d , mm (diameter of a coil)	19.0
b , mm (length of a coil)	40.0
N_t (number of turns)	10.0
d_0 , mm (diameter of a wire)	2.0
τ , mm (pitch of a helix)	4.0

Table 34: Final parameters of an RF resonator

3.2 Shaping the 3D model

With all dimensions in our hands we can start implementing them in a 3D design for the workshop. This section provides an overview of all parts used, their features and reasonings. One important feature to notice beforehand is the tunability. With the resonator as small as ours the chances that manufacturing complications would shift the target frequency further are rather high. In order to be able to vary it precisely the angular scale on the top cap (3.2.6) and the linear scale on the antenna mount (3.2.8) were designed.

3.2.1 RF resonator

Assembly of the RF resonator is shown on the figure 34. Every part is produced from oxygen-free copper to lower the resistivity. Colors are adjusted for a better perception.

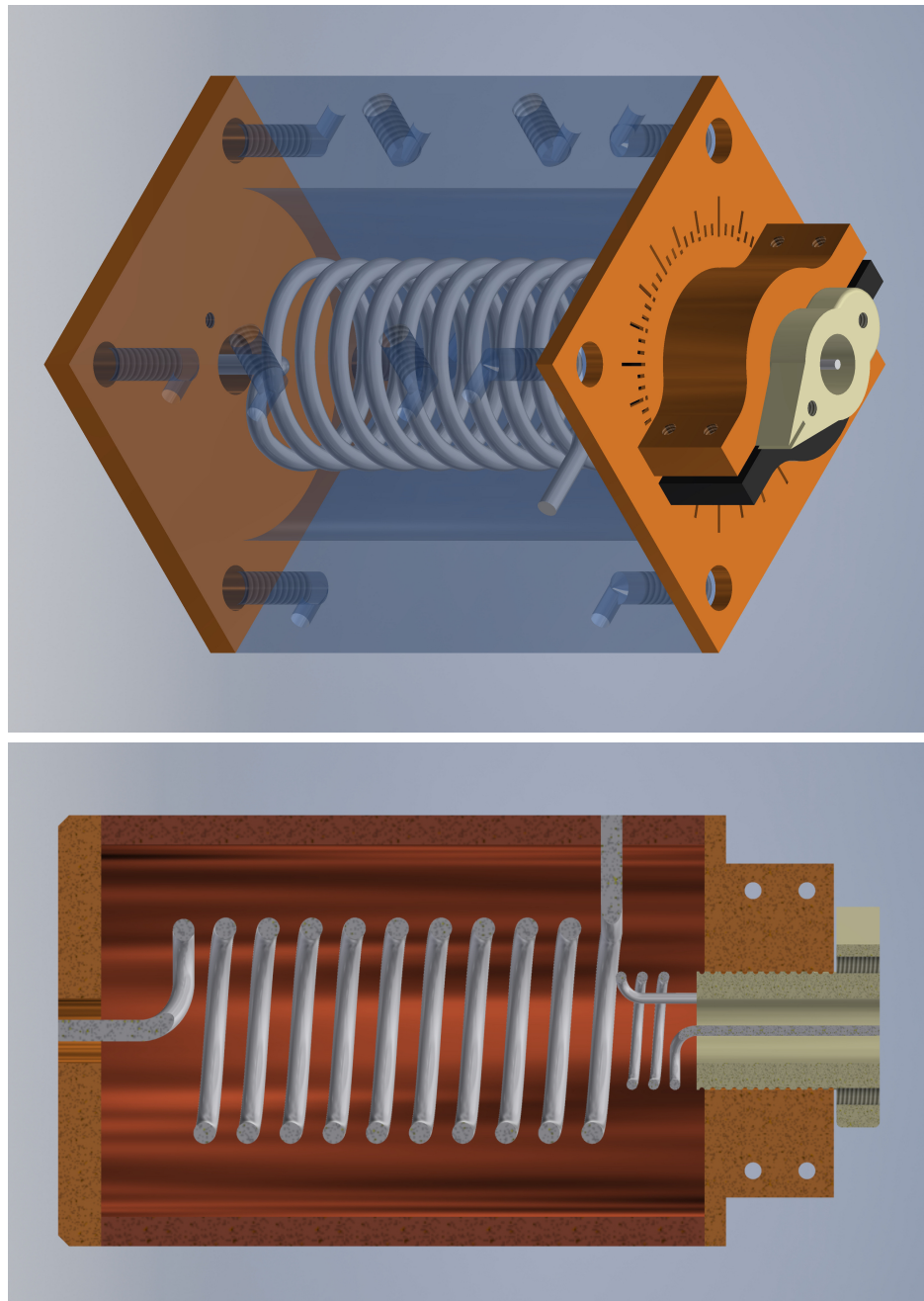


Figure 34: 3D model of an RF resonator

3.2. Shaping the 3D model

3.2.2 Bottom cap

Bottom cap as displayed in the figure 35 features:

- output hole for the helix (3.2.4)
- 4xM4 clearance holes to connect to the shield (3.2.3)
- 2xM2 thread holes for a SMA connector (RND 205-00499) for the helix (3.2.4)

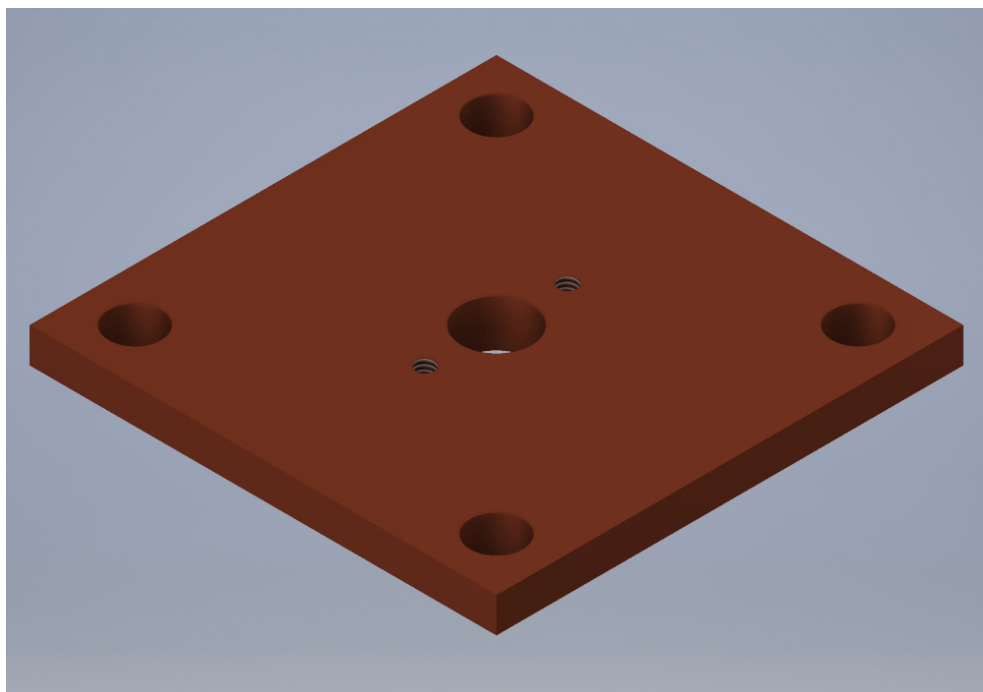


Figure 35: 3D model of a bottom cap

3.2.3 Shield

Shield as displayed in the figure 36 features:

- 4xM4 thread holes to connect to the top cap (3.2.6)
- 4xM4 thread holes to connect via a copper adapter to the top cover of the 4K chamber (figure 14)
- 4xM4 thread holes to connect to the bottom cap (3.2.2)
- 12x ventilation holes for M4 thread holes to avoid the slow leakage of the remaining air between the screw and the shield into the vacuum of the cryostat
- hole for the helix connection (3.2.4)

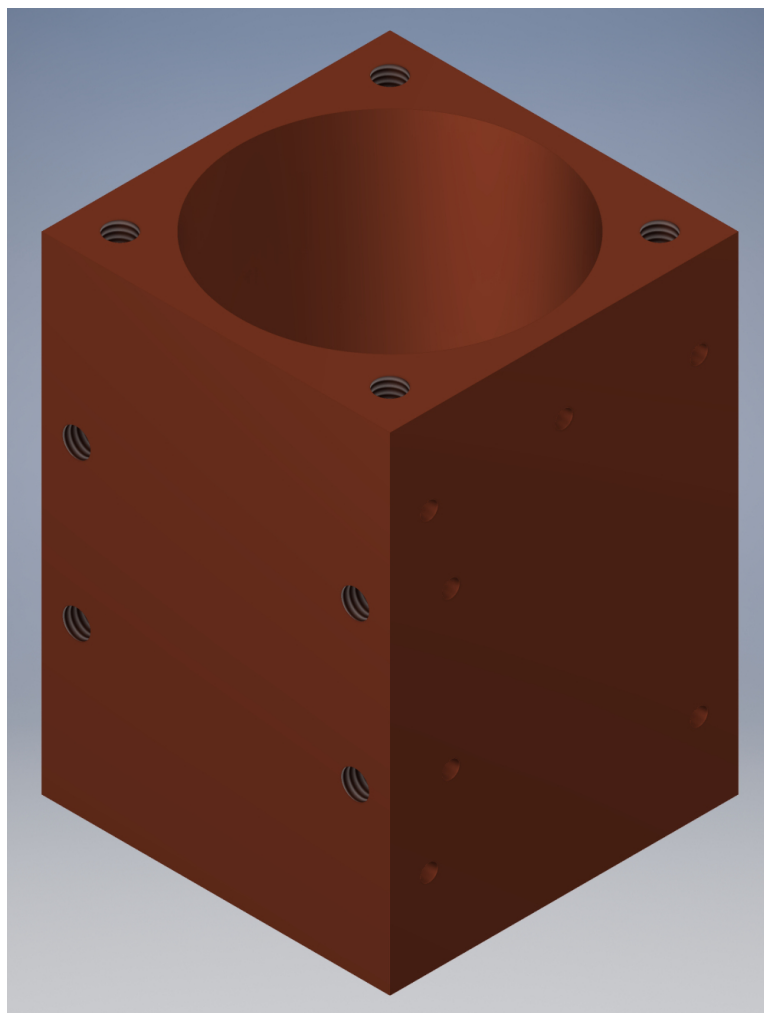


Figure 36: 3D model of a shield

3.2.4 Helix

Helix as displayed in the figure 37 features:

- end soldered to the shield (3.2.3)
- end soldered to a SMA (RND 205-00499) on the bottom cap (3.2.2)

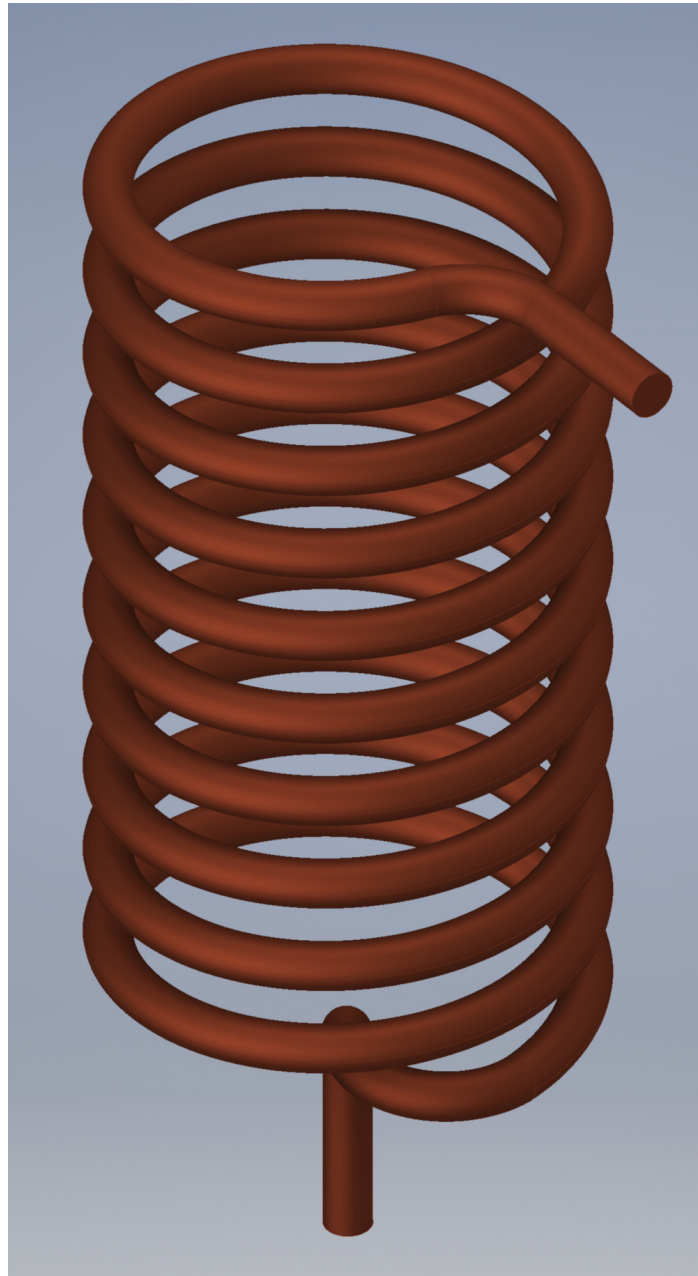


Figure 37: 3D model of a helix

3.2.5 Helix support

Since d_0 as specified in the table 34 is smaller than recommended thickness of 5 mm the question of mechanical stability arises. In order to eliminate potential mechanical oscillations we introduce a helix support made of PEEK to be inserted inside of the helix (3.2.4). PEEK was selected as a cryogenic compatible insulator thus minimizing its influence on the helix's inductivity.

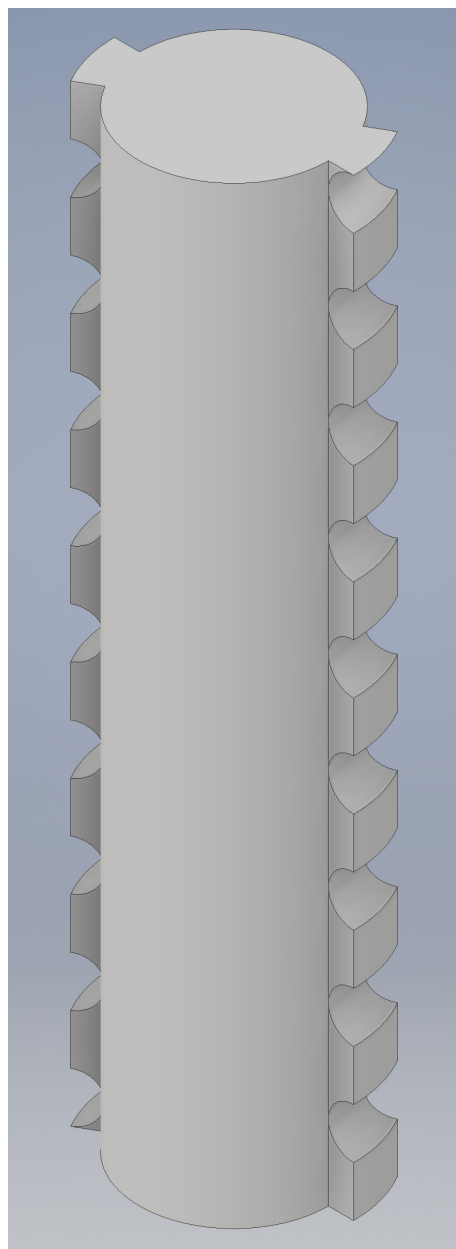


Figure 38: 3D model of a helix support

3.2.6 Top cap

Top cap as displayed in the figure 39 features:

- 4xM4 clearance holes to connect to the shield (3.2.3)
- 4xM2 thread holes to connect to the top cap clamp (3.2.7)
- tight hole for an antenna mount (3.2.8)
- angular scale for an antenna mount (3.2.8) as discussed in 3.2

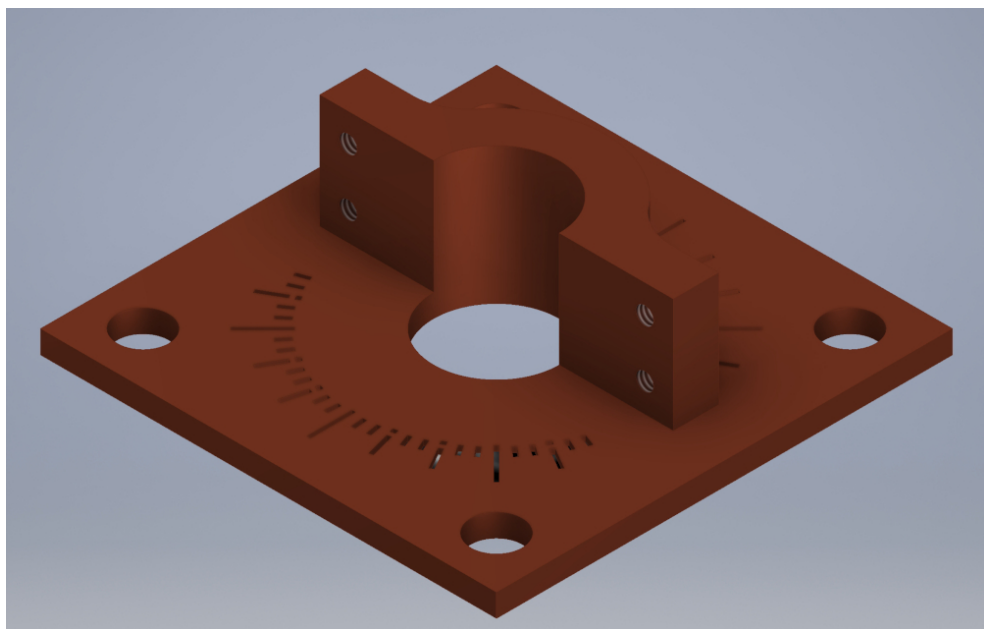


Figure 39: 3D model of a top cap

3.2.7 Top cap clamp

Top cap clamp as displayed in the figure 310 features:

- 4xM2 clearance holes to connect to the top cap (3.2.6)
- truncated semicircle to clamp an antenna mount (3.2.8)

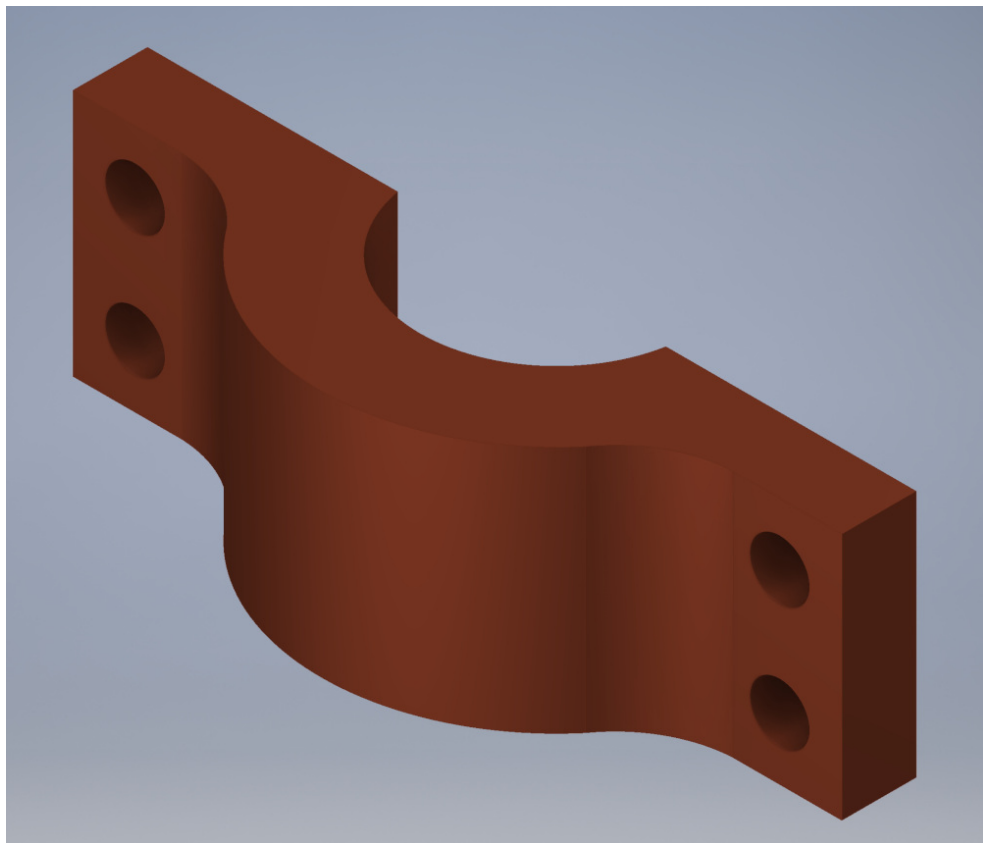


Figure 310: 3D model of a top cap clamp

3.2.8 Antenna mount

Antenna mount as displayed in the figure 311 features:

- 2xM2 thread holes for a SMA (RND 205-00499) connector for the antenna (3.2.9)
- hole for the antenna (3.2.9)
- cut for a precise usage of the angular scale on the top cap (3.2.6)
- 1 mm period cuts to determine the distance to the top cap (3.2.6) as discussed in 3.2

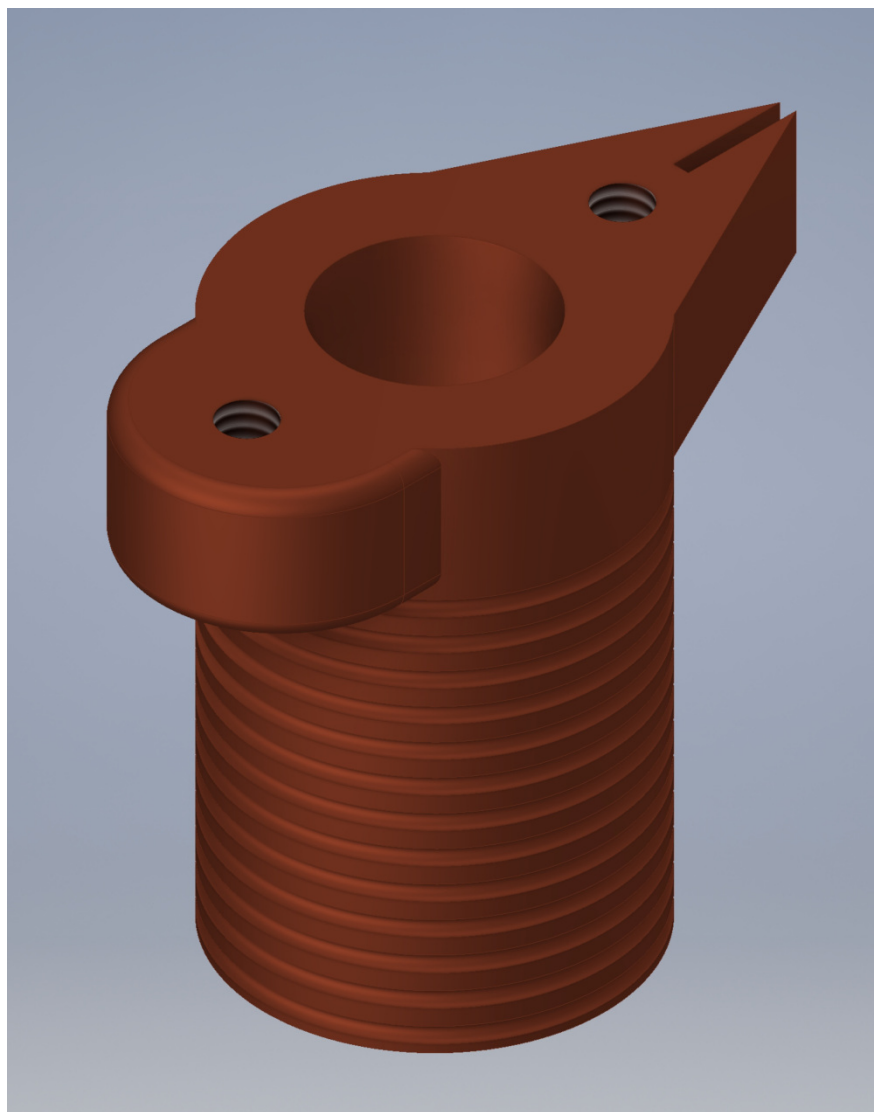


Figure 311: 3D model of an antenna mount

3.2.9 Antenna

Antenna as displayed in the figure 312 features:

- end connecting to a SMA (RND 205-00499) on the antenna mount (3.2.8)
- end soldered to the bottom of the antenna mount (3.2.8)
- using empirical estimation from [18] a diameter of 11 mm was selected



Figure 312: 3D model of an antenna

3.3 Final assembly

An overview of the assembled resonator can be seen in the figure 313.

Huge thanks to the ETH Workshop for their help in fitting the final apparatus into machinery constrains and for producing this delicate device.



Figure 313: Assembled resonator

Chapter 4

Validation

Two parameters defining the assembled resonator are the central frequency ω_0 and the quality factor Q . In this chapter we measure their experimental values and compare to those defined in the table 33.

4.1 Measurements

In order to determine ω_0 and Q we would take a look at the reflection spectrum of the system consisting of resonator + coaxial cable + capacitor. For every configuration the depth of the resonance was optimized by changing the distance and the angle between the antenna mount 3.2.8 and the top cap 3.2.6, effectively adjusting the antenna to coil coupling.

Parameter	Definition	Values	Units
C_{load}	External capacitive load	10, 15, 22	pF
L_{coax}	Length of the coaxial cable	10, 20, 50	cm

Table 41: Additional experimental parameters

At the time of writing there is no clear values for the capacitance of the trap and the length of the wires connecting it with the resonator. By using a set of parameters defined in the table 4.1 we aim to measure ω_0 and Q in the region similar to the one used for the numerical calculations and broad enough to include the point $\{C_{load} = C_{trap}; L_{coax}\}$ of the final setup.

- For $L_{coax} = 50$ two coaxial cables were connected, introducing 2 additional SMA connectors to the contour
- Available SMA connectors were of the male type. Unfortunately it is also the type commonly used for the wires, so we had to use an additional female-female adapter (+1 for $L_{coax} = 50$)

4.1. Measurements

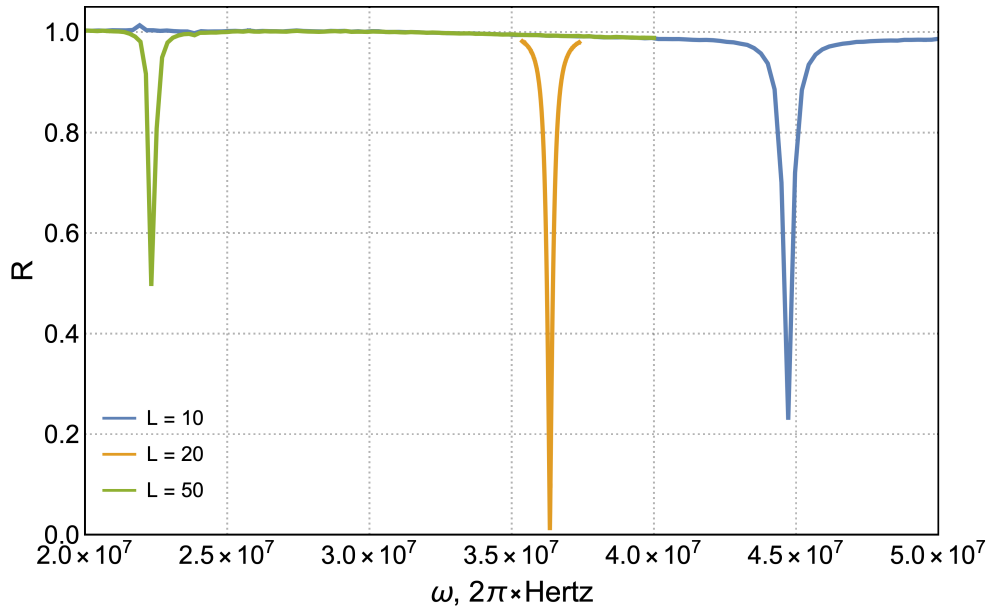


Figure 41: Reflection spectrum for $C = 10$

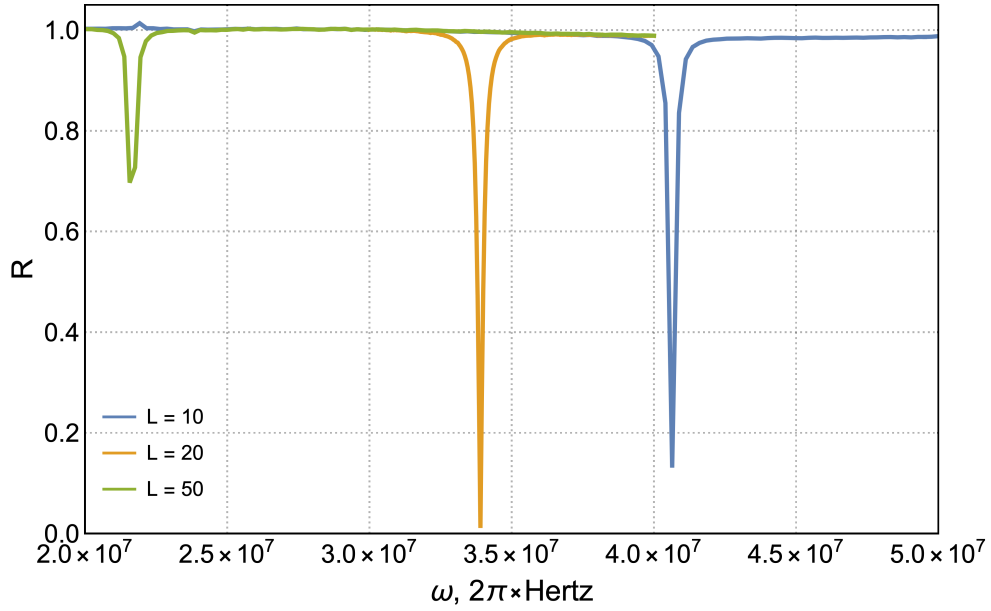
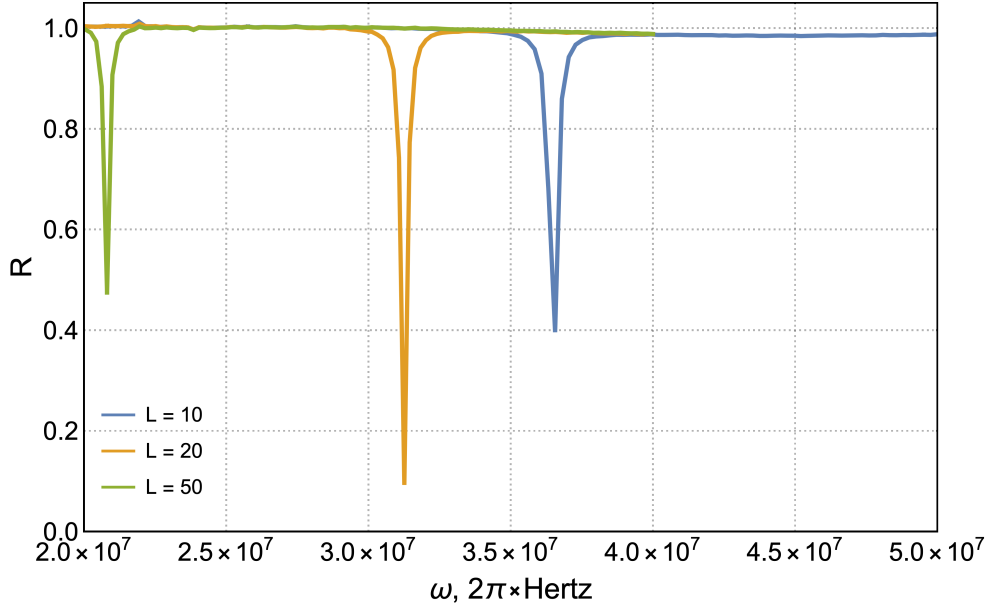


Figure 42: Reflection spectrum for $C = 15$


 Figure 43: Reflection spectrum for $C = 22$

4.2 Analysis

Finding ω_0 from experimental data is trivial, it is the central frequency of the peak. For the transmission spectrum Q can be defined as

$$Q = \frac{\omega_0}{\Delta\omega}, \quad (4.1)$$

where $\Delta\omega$ is the width of the peak at the $1/\sqrt{2}$ height. Since we are working with the reflection spectrum we need to adjust the height using the following expression

$$R_{1/\sqrt{2}} = 1 - \frac{1 - R_{peak}}{\sqrt{2}}. \quad (4.2)$$

Measured values of ω_0 and Q are presented in the table 4.2. Visual comparison with the predicted values from the table 33 is shown in the chart 4.2. $C_{load} = 22$ pF is not equal to the simulated $C_{trap} = 20$ pF but was considered being close enough. The closer experimental data is to the point $\{0; 0\}$ the better it reflects the simulations. It can be seen that increased capacitance due to both C_{load} and L_{coax} tends to increase deviations from predictions. Our model does not account for the additional capacitances and resistances of the SMA connectors and the wires. Thus the predicted values in the table 4.2 are expected to be independent of the wire length and the number of SMA connectors with “—||—” standing for the “same as above”.

4.3. Ideal drive

C_{load} , pF	L_{coax} , cm	ω_0^{simul} , $2\pi * \text{MHz}$	ω_0 , $2\pi * \text{MHz}$	Q^{simul}	Q
10	10	44.6	44.7	418	223.5
10	20	— —	36.3	— —	269.9
10	50	— —	22.3	— —	140.4
15	10	45.6	40.6	360	216.5
15	20	— —	33.9	— —	268.6
15	50	— —	21.6	— —	69.7
22	10	46.9	36.5	311	153.5
22	20	— —	31.2	— —	192.3
22	50	— —	20.8	— —	145.6

Table 42: Measured Q and ω_0 for various configurations

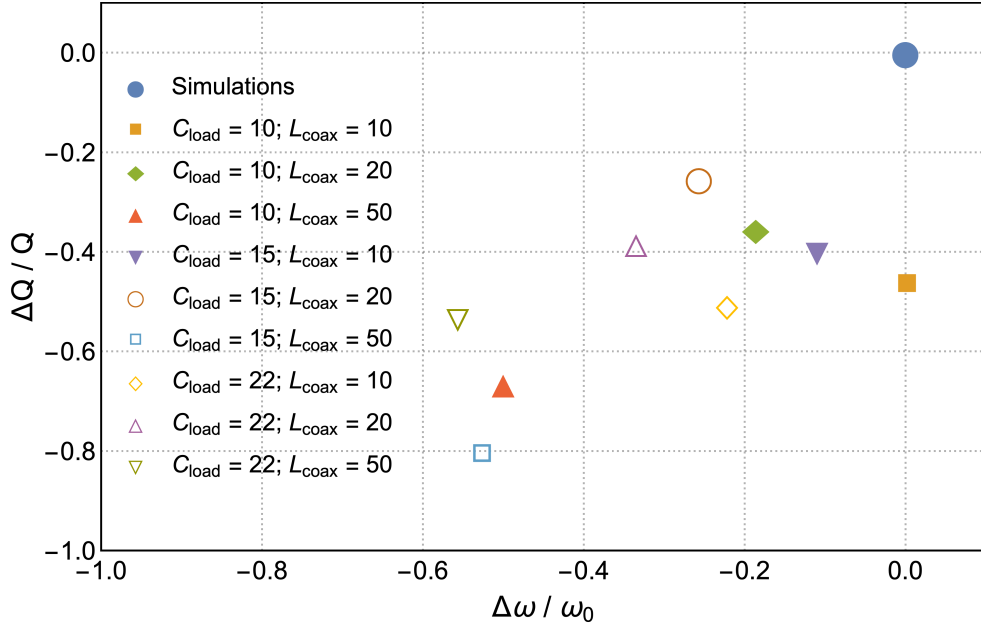


Figure 44: Relative deviations of Q and ω_0

4.3 Ideal drive

This section includes simulations of the ideal drive for a 300 and 320 V drive by Chiara Decaroli, figures 4.3 and 4.3 respectively. Let's take a look at the figure 4.3. If the resonator frequency is below $\approx 2\pi * 34$ MHz the ion trap becomes unstable. On the other hand, with frequencies larger than $\approx 2\pi * 39$ MHz the secular frequency of the ion itself drops below $2\pi * 6$ MHz which does not allow certain quantum operations. Thus it is desired for the ω_0 to belong to the intersection of the white areas. We show what measured points respect this condition in the table 4.3.

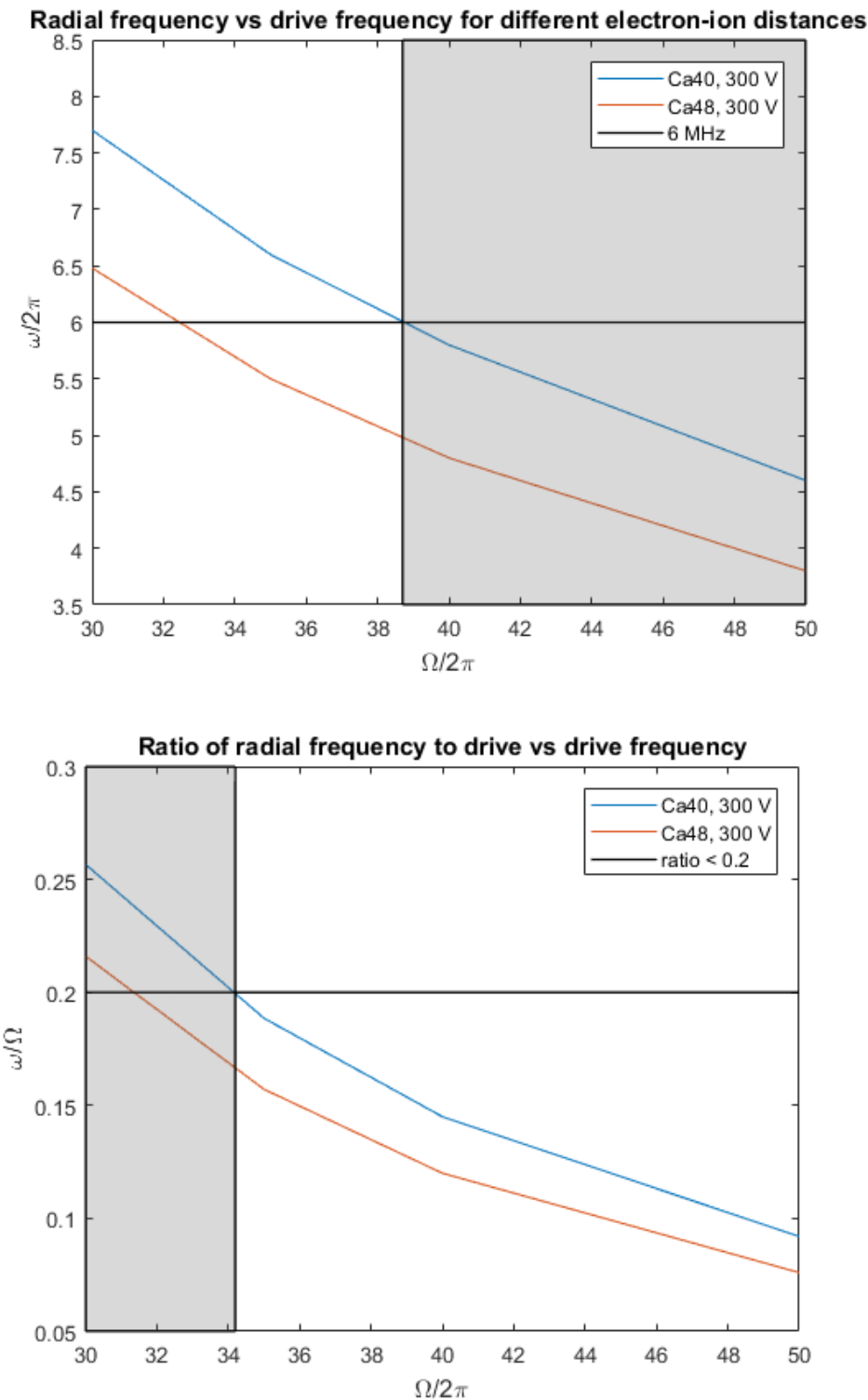


Figure 45: Simulation of the ideal drive for 300V

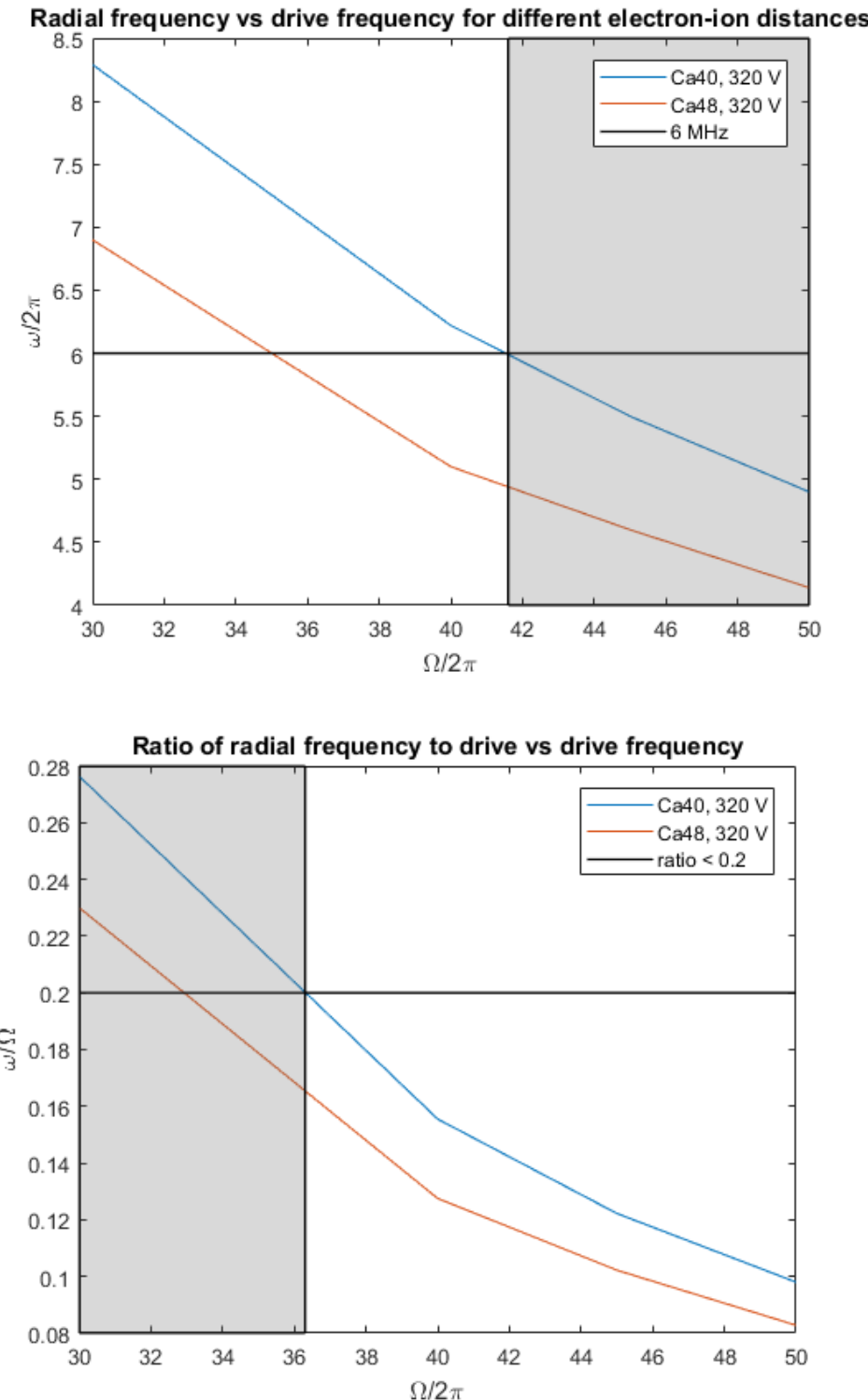


Figure 46: Simulation of the ideal drive for 320V

C_{load} , pF	L_{coax} , cm	Compatible with 300V	Compatible with 320V
10	10	✗	✗
10	20	✓	✓
10	50	✗	✗
15	10	✗	✓
15	20	✓	✗
15	50	✗	✗
22	10	✓	✓
22	20	✗	✗
22	50	✗	✗

Table 43: Fitting the experimental data into the ion trap constrains

4.4 Power dissipation

Since the experiment would run in a cryogenic environment it is crucial to estimate the dissipated power to find out whether a cryostat should be able to handle it. According to [13] average dissipated power P can be written as

$$P = \frac{I_0^2 R}{2} = \frac{(U_0 \omega_0 C)^2 R}{2} = \frac{U_0^2}{2 \omega_0 Q L} \quad (4.3)$$

with a peak current I_0 , peak voltage U_0 , inductance of the resonator L , and capacitance of the system C . Since in the section 4.1 we made measurements with various known values of a capacitive load it is possible to give an estimation of $L = 600$ nH. By picking the values from the table 4.3 that are compatible with $U_0 = 300$ or 320V we present results for the needed input power in the table 4.4.

C_{load} , pF	L_{coax} , cm	U_0 , V	P , W
10	20	300	1.20
10	20	320	1.37
15	10	320	1.53
15	20	300	1.30
22	10	300	2.11
22	10	320	2.40

Table 44: Estimated input power P for various configurations

4.5 Voltage gain

We would also like to know what kind of an input signal should be provided to the resonator to successfully operate an ion trap. By taking a quick look

4.5. Voltage gain

at [13] we can define the voltage gain as given by the absolute of the transfer function like the following:

$$G(\omega) = \left| \frac{U_0(\omega)}{U_i(\omega)} \right| = \left| \frac{1 / (i\omega C)}{R + i\omega L + 1 / (i\omega C)} \right| = \frac{\omega_0^2}{\sqrt{(\omega^2 - \omega_0^2)^2 + (\omega\omega_0/Q)^2}} \quad (4.4)$$

Most likely we would like to operate the trap in the resonant mode in which $\omega = \omega_0$ and thus $G = G(\omega_0) = Q$. However in some scenarios it might be beneficial to select a different frequency. In order to describe this case we have used the equation 4.4 to plot $G(\omega)$ for all configurations from the table 4.3 where ω_0 already belongs to the approximate desired joint interval of the $2\pi * 34 - 2\pi * 42$ MHz. Results can be seen in the figure 4.5.

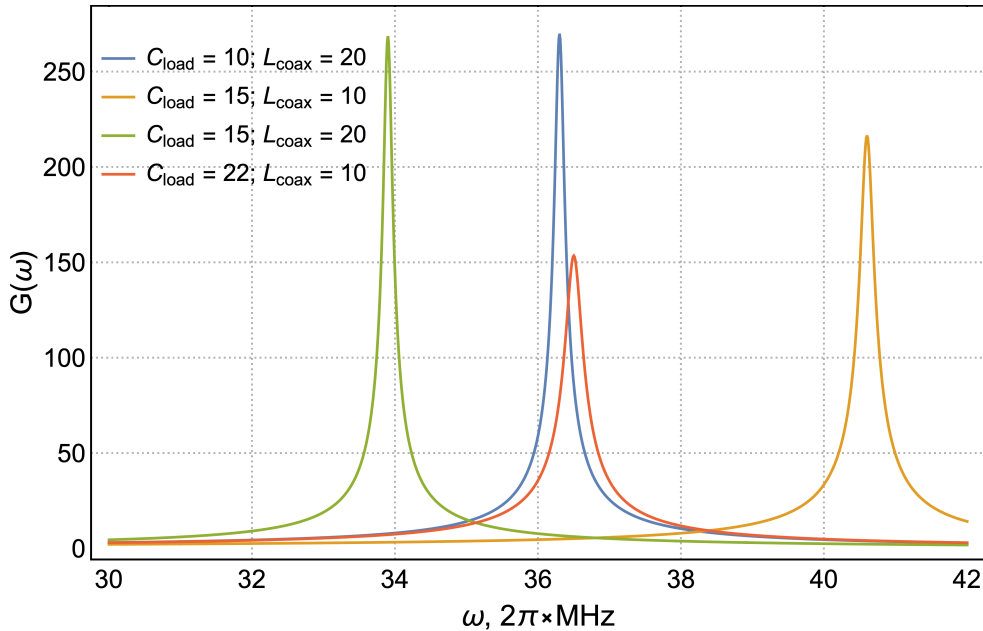


Figure 47: Plot of $G(\omega)$ for various configurations

Chapter 5

Results

The aim of this project was to create an RF helical resonator to support an ion trap. This goal was successfully achieved. As a result we were able to design, produce, and validate a delicate helical resonator with reasonable Q and ω_0 values. However a watchful reader can rightfully point out that those do not correspond exactly to the predictions. Let us provide a short analysis of the potential reasons that could lead to that:

- Resonance frequency is not exactly $2\pi * 40$ MHz because algorithm provided in the appendix B only allows to select values in the vicinity of the target frequency. We have used the $\pm 15\%$ frequency margin
- Helical resonator has spent a fair share of time being in contact with air between production and validation phases which has led to oxidation of the copper thus effectively increasing the resistivity of the skin layer
- Q and ω_0 were measured at the room temperature while the theoretical model has operated with the resistivity in the cryogenic environment
- Calculations have not accounted for the additional capacitance and resistance introduced by the SMA connectors and external wires
- Distance tuning almost didn't work, for an optimal tuning the distance between the antenna mount and the top cap was kept close to 0

Chapter 6

Outlook

In this chapter we would respond to the issues lifted by the chapter 5 and share tips for the future similar projects.

- Ideally initial ω_0 for the algorithm defined in the appendix A should be picked as a middle value in the intervals discussed in the section 4.3. Afterwards in the appendix B instead of a percentage frequency margin we check whether the resulting frequency belongs to the corresponding interval.
- Cleaning the outer oxide layer by sanding or acid and placing the resonator into the cryostat should lower the resistivity of the skin layer thus improving Q [13, 3]
- Model should account better for the SMA connectors and wires. Just like with the trap capacitance, approximate values should be used for the calculations
- Removing additional capacitance and resistance by soldering the non-coaxial cable directly to the shield might yield better results
- In order to improve the distance-based tuning the length of the antenna mount can be increased and/or antenna should contain more turns to strengthen the antenna to coil coupling
- Lack of the angular tuning means that the resonator was produced with high precision since it shows that the system has a circular symmetry. However this can be also verified without the angular scale, which allows us to drop it in the new designs

Chapter 7

Conclusion

This project shows that in principle it is possible to produce a reasonably small and efficient helical resonator for the ion trap. However the mechanical and assembly challenges would advise to evaluate the available resonator options carefully when designing for a comparable or smaller volume.

If you are reading this, you got to the end of the main part of my report! I hope that it helped you to understand the theory behind the helical resonators and gave an idea of how one could get the maximum Q and the closest to targeted ω_0 out of the provided setup. I wish you best of luck in using this knowledge for your aims.

Appendix A

Mathematica code for Macalpine's model

This is a relevant part of the script supporting calculations in [13].

```
In[1]:= (* Physical Constants and Units *)
μ0 = 4*π*10-7;
ε0 = 8.854187817*10-12;
c = 299792458;
AMU = 1.6605402*10-27;
h = 6.6260755*10-34;
ℏ =  $\frac{h}{2\pi}$ ;
μB = 9.2740154*10-24;
kB = 1.380658*10-23;
grav = 9.8;
a0 = 0.5291772108*10-10;
me = 9.1093826*10-31;
ee = 1.60217733*10-19; eV = ee;
Eh =  $\frac{\hbar^2}{me a_0^2}$ ;
m=1; μm=10-6m; mm=10-3m; cm=10-2m; nm=10-9m; km=103m;
in=2.54cm; ft=12in; mi=5280*ft;
K=1; mK=10-3K; μK=10-6; nK=10-9K; pK=10-12;
T=1; mT=10-3K; G=10-4; mG=10-3G; μG=10-6;
sec=1; s=1; ms=10.0-3s; μs=10-6s; ns=10-9s;
Ω=1; mΩ=10-3; kΩ=103; MΩ=106;
A=1; mA=10-3A; μA=10-6; nA=10-9;
W=1; mW=10-3; μW=10-6; nW=10-9;
Hz=1; kHz=103; MHz=106; GHz=109;
nF=10-9; pF=10-12;
nH=10-9; pH=10-12;
```

```

In[2]:= (* Calculations for Cu resonator *)
Ds[Bs_]:= 0.75Bs; (*diameter of shield*)
d[Bs_]:= 0.55Ds[Bs]; (*diameter of helix*)
b[Bs_]:= 1.5d[Bs]; (*length of helix*)

Nt[Bs_,f0_]:=  $\frac{48.26 \cdot 10^6}{f0 \cdot Ds[Bs]}$ ; (*number of turns*)
d0[Bs_,f0_]:= 0.5  $\frac{b[Bs]}{Nt[Bs, f0]}$ ; (*diameter of wire*)
 $\tau[Bs_, f0_] := \frac{b[Bs]}{Nt[Bs, f0]}$ ; (*pitch*)

(*effective inductance*)
Leff[Bs_,f0_]:=  $9.84 \cdot 10^{-7} \cdot \left( \frac{Nt[Bs, f0] \cdot d[Bs]}{b[Bs]} \right)^2 \cdot \left( 1 - \left( \frac{d[Bs]}{Ds[Bs]} \right)^2 \right)$ ;
Ceoff[Bs_]:=  $\frac{2.95 \cdot 10^{-11}}{\log_{10} \frac{Ds[Bs]}{d[Bs]}}$ ; (*effective capacitance*)

Z0[Bs_,f0_]:=  $\sqrt{\frac{Leff[Bs, f0]}{Ceoff[Bs]}}$ ; (*characteristic impedance*)
v[Bs_,f0_]:=  $\frac{1}{\sqrt{Leff[Bs, f0] \cdot Ceoff[Bs]}}$ ; (*velocity*)
 $\lambda[Bs_, f0_] := \frac{v[Bs, f0]}{f0}$ ; (*wavelength*)

Q[Bs_,f0_]:= 1.97 Ds[Bs]  $\sqrt{f0}$ ;

omega[Bs_,f0_,Cl_]:= Module[{w},
  w =  $v/.FindRoot[\frac{1}{2\pi \cdot Z0[Bs, f0] \cdot Cl \cdot v} == \tan(\frac{2\pi v \cdot b[Bs]}{v[Bs, f0]})]$ , {v, f0}] [[1]];
  Return@w;
]

In[3]:= Bs = 60mm; (*length of shield*)
(* This frequency needs to be varied
until loaded frequency is close to target frequency*)
f0 = 97.023MHz; (*center frequency*)
Cl = 10pF; (*trap capacitance*)

Print["Bs = ", Bs/mm, " mm (length of shield)"]
Print["Ds = ", Ds[Bs]/mm, " mm (diameter of shield)"]
Print["d = ", d[Bs]/mm, " mm (diameter of helix)"]
Print["b = ", b[Bs]/mm, " mm (length of helix)"]
Print["Nt = ", Nt[Bs,f0], " (number of turns)"]
Print["d0 = ", d0[Bs,f0]/mm, " mm (diameter of wire)"]

```

```

Print["τ = ",τ[Bs,f0]/mm," mm (pitch of helix)"]
Print["Z₀ = ",Z₀[Bs,f0]/ω," ω (characteristic impedance)"]
Print["Lᵅᵅᵅ = ",Lᵅᵅᵅ[Bs,f0]/(nH/mm)," nH/mm (effective inductance)"]
Print["Cᵅᵅᵅ = ",Cᵅᵅᵅ[Bs]/(pF/mm)," pF/mm (effective capacitance)"]
Print["v = ",v[Bs,f0]/(m/s)," m/s (velocity)"]
Print["λ = ",λ[Bs,f0]/mm," mm (wavelength)"]
Print["f₀ = ",f₀/MHz," MHz (unloaded frequency)"]
Print["Q = ",Q[Bs,f0]," (quality factor)"]
Print["ν₀ = ",omega[Bs,f0,C1]/MHz," MHz (loaded frequency)"]

Clear[Bs,f0,C1];
Bs = 60 mm (length of shield)
Ds = 45. mm (diameter of shield)
d = 24.75 mm (diameter of helix)
b = 37.125 mm (length of helix)
Nt = 11.0535 (number of turns)
d₀ = 1.67933 mm (diameter of wire)
τ = 3.35866 mm (pitch of helix)
Z₀ = 572.731 Ω (characteristic impedance)
Lᵅᵅᵅ = 37.2698 nH/mm (effective inductance)
Cᵅᵅᵅ = 0.11362 pF/mm (effective capacitance)
v = 1.53672*10^7 m/s (velocity)
λ = 158.387 mm (wavelength)
f₀ = 97.023 MHz (unloaded frequency)
Q = 873.205 (quality factor)
ν₀ = 40. MHz (loaded frequency)

```

Appendix B

Mathematica code for Siversns' model

Following calculations are heavily based on a script generously provided by James David Siversns. All variables and references correspond to [18].

```
In[1]:= (* Units and constants *)
MHz = 106;
pF = 10-12;
Ω = 1;
mm = 10-3;
m = 1;
H = 1;
μ0 = 4π*10-7;

In[2]:= (* Trap and wire values *)
Cw = 0.00001 pF; (* Wire to trap capacitance *)
Rt = 0.1 Ω; (* Trap resistance *)
CΣ[Ct_] := Cw + Ct; (* Sum of above *)

In[3]:= calculateQ[dMillimeters_, γ_]:=Module[{
(* Arguments naming as in Siversns paper *)
d0, τ, d, De, α, ρ, eN, b, Cc, KLC, KCs, Cs, LC, ω0, δ, lc, r, Ns, ls, a,
Rs, Rc, Rj, XLc, XCc, Xct, Xcw, XCs, Zcoil, ZE, Ztot, RealZ, Q,
maxSize, log, ωRes, Capacitance
},
Capacitance = 20pF;
(* Switch log function for plotting *)
log = Print;
log = (#)&

(* Resonator parameters *)
(* Coil wire diameter, we take it from Macalpine *)
d0 = 1.95mm;
```

```

 $\tau = 2*d0$ ; (* Winding pitch *)
 $d = d\text{Millimeters}*\text{mm}$ ; (* Diameter of coil *)
 $De = d/\gamma$ ; (* Diameter of a shield *)
 $\alpha = d/De$ ;
(* Resistivity of resonator material *)
 $\rho = 1.7*10^{-8}*\Omega*\text{m}$ ;
(* Given by the 4K chamber design *)
maxSize = 36mm;
b = 56mm - De/2;
(* Handling case of a too large resonator *)
If[d>maxSize || De>maxSize || b<=0, Return@0];

log["b = ", b/mm, "mm"];
log["d = ", d/mm, "mm"];
log["D = ", De/mm, "mm"];

eN = b/tau; (* Number of turns in the coil *)
log["N = ", eN];
(* Coil self capacitance - equation 25 *)

Cc = ((11.26  $\frac{b}{d}$ ) + 8 + ( $\frac{27}{\sqrt{\frac{b}{d}}}$ ))d pF;

KLC = 39.37  $\frac{0.025 \left(\frac{d}{\tau}\right)^2 (1-\alpha^2)}{\left(\frac{d}{\tau}\right)^2}$  10-6 H/m;
KCs = 39.37  $\frac{0.75}{\text{Log}[10, \frac{1}{\alpha}]}$  pF/m;

(* Shield-coil capacitance - equation 26 *)
Cs = b KCs;
(* Inductance of coil inside a shield - equation 27 *)
LC = b KLC;
(* Resonant frequency - equation 21 *)
 $\omega_{\text{Res}}[Ct_] := \frac{1}{\sqrt{(Cs+Ct+Cw+Cc)LC}}$ ;
log[" $\omega$  = ", omegaRes[Capacitance]/(2π MHz), "MHz"];

ω0[Ct_] := 2π*40 MHz; (* This is a target frequency *)
(* Allowing 15% accuracy for the frequency *)
If[
     $\frac{\text{Abs}[\omega_0[\text{Capacitance}] - \omega_{\text{Res}}[\text{Capacitance}]]}{\omega_0[\text{Capacitance}]}$  > 0.15,
    Return@0
];

```

```

δ[Ct_] := Sqrt[ $\frac{2 \rho}{(\omega_0[Ct] \mu_0)}$ ]; (* Skin depth *)
(* Unwound length of the coil *)
lc =  $2\pi \sqrt{\left(\frac{d}{2}\right)^2 + \left(\frac{\tau}{2\pi}\right)^2} \frac{b}{\tau}$ ;
r =  $\frac{d}{2} \left(\frac{1}{\alpha} - 1\right)$ ;
(* Number of "turns" in the currents path in the shield
- equation 31 *)
Ns =  $\frac{b \ lc}{4\pi r^2}$ ;
(* Distance of current path in the shield - equation 32 *)
ls = Ns Sqrt[ $\pi^2 \left(\frac{d}{\alpha}\right)^2 + \left(\frac{b}{Ns}\right)^2$ ];
Rs[Ct_] :=  $\frac{\rho \ ls}{b \ \delta[Ct]}$ ;
Rc[Ct_] :=  $\frac{\rho \ lc}{d_0 \ \pi \ \delta[Ct]}$ ;
(* Resistance of solder joint as a function of frequency -
the 0.003 is the DC resistance of a typical solder joint
between shield and coil, however this can vary
and is best to measure *)
Rj[Ct_] := 0.003 Sqrt[ $\frac{\omega_0[Ct]}{2\pi \cdot 10^5}$ ] Ω;
(* Q calculations *)
XLc[Ct_] := ω0[Ct] LC;
XCc[Ct_] :=  $\frac{1}{\omega_0[Ct] Cc}$ ;
Xct[Ct_] :=  $\frac{1}{\omega_0[Ct] Ct}$ ;
Xcw[Ct_] :=  $\frac{1}{\omega_0[Ct] Cw}$ ;
XCs[Ct_] :=  $\frac{1}{\omega_0[Ct] Cs}$ ;
Zcoil[Ct_] :=  $\left( \frac{1}{(i \ XLc[Ct] + Rc[Ct])} + \frac{1}{\frac{1}{i} XCc[Ct]} \right)^{-1}$ ;
ZE[Ct_] :=  $\left( \frac{1}{\left(\frac{1}{i} Xct[Ct] + Rj[Ct]\right)} + \frac{1}{\frac{1}{i} Xcw[Ct]} + \frac{1}{\frac{1}{i} XCs[Ct]} \right)^{-1}$ ;
Ztot[Ct_] := Zcoil[Ct] + ZE[Ct] + Rs[Ct] + Rj[Ct];

```

```

RealZ[Ct_] := 
$$\frac{\frac{Rc[Ct] \ XCc[Ct]^2}{Rc[Ct]^2 + (XCc[Ct] - XLc[Ct])^2} +$$


$$\frac{Rt \ XCs[Ct]^2 \ Xcw[Ct]^2}{Rt^2(XCs[Ct] + Xcw[Ct])^2 + (XCs[Ct](Xct[Ct] + Xcw[Ct]) + Xct[Ct]Xcw[Ct])^2}$$


$$+ \ Rs[Ct] + Rj[Ct];$$


Q[Ct_] := 
$$\frac{LC \ \omega_0[Ct]}{RealZ[Ct]};$$


Return@Q[Capacitance];
]

In[4]:= SetDirectory[NotebookDirectory[]];
contourData = Table[
  {γ, d, calculateQ[d, γ]},
  {d, 15, 25, 0.01},
  {γ, 0.4, 0.7, 0.01}
] // Flatten[#, 1]&

ListContourPlot[
  contourData,
  PlotLegends → Automatic,
  FrameLabel → {"d/D", "d, mm"}
]

In[5]:= (* Final parameters *)
calculateQ[19, 0.55]

b = 38.7273mm
d = 19mm
D = 34.5455mm
N = 9.93007
ω = 39.7919MHz

Out[5]= 362.188

```

Bibliography

- [1] K. Deng, Y. L. Sun, W. H. Yuan, Z. T. Xu, J. Zhang, Z. H. Lu, and J. Luo. A modified model of helical resonator with predictable loaded resonant frequency and Q-factor. *Review of Scientific Instruments*, 85(10):1–8, 2014.
- [2] Paul A. M. Dirac. On the Theory of Quantum Mechanics. *Proceedings of the Royal Society A: Mathematical, Physical and Engineering Sciences*, 112(762):661–677, oct 1926.
- [3] Matteo Fadel. Cryogenic Setup for Fast Manipulation of the Quantum Motional States of Trapped Ions. *Masters Thesis*, 2013.
- [4] Richard Phillips Feynman. The Wonders That Await a Micro-Microscope. *The Saturday Review*, pages 45–47, 1960.
- [5] Davide Gandolfi. *Compact RF Amplifier for Scalable Ion-Traps*. PhD thesis, Università degli Studi di Trento and Universität Innsbruck, 2010.
- [6] Amy Greene. *Experiments Towards Mitigation of Motional Heating in Trapped Ion Quantum Information Processing*. Master of engineering in electrical engineering and computer science thesis, Massachusetts Institute of Technology, 2016.
- [7] S. Gulde. *Experimental realization of quantum gates and the Deutsch-Josza algorithm with trapped ^{40}Ca -ions*. PhD thesis, University of Innsbruck, 2017.
- [8] K G Johnson, J. D. Wong-Campos, A Restelli, K A Landsman, B Neyenhuis, J Mizrahi, and C. Monroe. Active stabilization of ion trap radiofrequency potentials. *Review of Scientific Instruments*, 87(5):053110, may 2016.

Bibliography

- [9] T. Karin, I. Le Bras, A. Kehlberger, K. Singer, N. Daniilidis, and H. Häffner. Transport of charged particles by adjusting rf voltage amplitudes. *Applied Physics B*, 106(1):117–125, jan 2012.
- [10] Ezra Kassa, Hiroki Takahashi, Costas Christoforou, and Matthias Keller. Precise positioning of an ion in an integrated Paul trap-cavity system using radiofrequency signals. *Journal of Modern Optics*, 65(5-6):520–528, mar 2018.
- [11] Ezra M. B. Kassa. *Single ion coupled to a high-finesse optical fibre cavity for cQED in the strong coupling regime*. Doctor of philosophy thesis, University of Sussex, 2016.
- [12] Muir Kumph. *2D Arrays of Ion Traps for Large Scale Integration of Quantum Information Processors*. PhD thesis, University of Innsbruck, 2015.
- [13] Florian Michael Leupold. *Bang-bang Control of a Trapped-Ion Oscillator*. PhD thesis, ETH Zurich, 2015.
- [14] W. Macalpine and R. Schildknecht. Coaxial Resonators with Helical Inner Conductor. *Proceedings of the IRE*, 47(12):2099–2105, dec 1959.
- [15] Wolfgang Paul. Electromagnetic Traps for Charged and Neutral Particles(Nobel Lecture). *Angewandte Chemie International Edition in English*, 29(7):739–748, jul 1990.
- [16] A.M. Prokhorov. Joule–Lenz law. *Great Soviet Encyclopedia*, 1972.
- [17] Felix Rohde. *Remote ion traps for quantum networking: Two-photon interference and correlations*. Dissertation, ICFO Barcelona, 2009.
- [18] J. D. Sivers, L. R. Simkins, S. Weidt, and W. K. Hensinger. On the application of radio frequency voltages to ion traps via helical resonators. *Applied Physics B*, 107(4):921–934, jun 2012.
- [19] Q. A. Turchette, Kielpinski, B. E. King, D. Leibfried, D. M. Meekhof, C. J. Myatt, M. A. Rowe, C. A. Sackett, C. S. Wood, W. M. Itano, C. Monroe, and D. J. Wineland. Heating of trapped ions from the quantum ground state. *Physical Review A*, 61(6):063418, may 2000.
- [20] Andre J. S. Van Rynbach. *Microfabricated Surface Trap and Cavity Integration for Trapped Ion Quantum Computing by Abstract Microfabricated Surface Trap and Cavity Integration for Trapped Ion Quantum Computing*. Doctor of philosophy dissertation, Graduate School of Duke University, 2016.

Declaration of originality

The signed declaration of originality is a component of every semester paper, Bachelor's thesis, Master's thesis and any other degree paper undertaken during the course of studies, including the respective electronic versions.

Lecturers may also require a declaration of originality for other written papers compiled for their courses.

I hereby confirm that I am the sole author of the written work here enclosed and that I have compiled it in my own words. Parts excepted are corrections of form and content by the supervisor.

Title of work (in block letters):

Authored by (in block letters):

For papers written by groups the names of all authors are required.

Name(s):

First name(s):

With my signature I confirm that

- I have committed none of the forms of plagiarism described in the '[Citation etiquette](#)' information sheet.
- I have documented all methods, data and processes truthfully.
- I have not manipulated any data.
- I have mentioned all persons who were significant facilitators of the work.

I am aware that the work may be screened electronically for plagiarism.

Place, date

Signature(s)

For papers written by groups the names of all authors are required. Their signatures collectively guarantee the entire content of the written paper.